JOURNAL OF GEOPHYSICAL RESEARCH, VOL. 104, NO. D17, PAGES 21,549–21,568, SEPTEMBER 20, 1999

Observations of convective and dynamical instabilities in tropopause folds and their contribution to stratosphere-troposphere exchange

John Y. N. Cho,[1] Reginald E. Newell,[1] T. Paul Bui,[2] Edward V. Browell,[3] Marta A. Fenn,[4] Michael J. Mahoney,[5] Gerald L. Gregory,[3] Glen W. Sachse,[3] Stephanie A. Vay,[3] Tom L. Kucsera,[6] and Anne M. Thompson[6]

Abstract. With aircraft-mounted in situ and remote sensing instruments for dynamical, thermal, and chemical measurements we studied two cases of tropopause folding. In both folds we found Kelvin-Helmholtz billows with horizontal wavelength of ~900 m and thickness of ~120 m. In one case the instability was effectively mixing the bottomside of the fold, leading to the transfer of stratospheric air into the troposphere. Also, we discovered in both cases small-scale secondary ozone maxima shortly after the aircraft ascended past the topside of the fold that corresponded to regions of convective instability. We interpreted this phenomenon as convectively breaking gravity waves. Therefore we posit that convectively breaking gravity waves acting on tropopause folds must be added to the list of important irreversible mixing mechanisms leading to stratosphere-troposphere exchange.

1. Introduction

At midlatitudes, tropopause folds are believed to be the major source of stratosphere-to-troposphere transfer of air. These V-shaped layers with high ozone and potential vorticity content angle down from the stratosphere for several kilometers and, at times, reach the planetary boundary layer. However, the fold itself is a reversible process, so for permanent stratosphere-troposphere exchange to take place the air in the fold must mix irreversibly with the outside environment. This necessary mixing has been attributed to Kelvin-Helmholtz-induced turbulence [*Shapiro*, 1980], boundary layer turbulence [*Johnson and Viezee*, 1981], stratospheric streamer fragmentation and roll up [*Appenzeller et al.*, 1996], and localized wet convection [*Langford and Reid*, 1998]. However, few direct observations of the exchange process exist, and it is far from clear which, if any, of these proposed mixing mechanisms is dominant.

In this paper we present observations made through two tropopause folds with in situ and remote sensing instruments aboard a DC-8 during the NASA Subsonics Assessment (SASS) Ozone and Nitrogen Experiment (SONEX) [*Singh et al.*, 1999]. Although the primary purpose of this mission was not the study of stratosphere-troposphere exchange, the extensive collection of chemical, dynamical, and thermal measurements in the upper troposphere enabled us to examine examples of tracer transport around tropopause folds.

2. Instrument Descriptions

SONEX was conducted between October 7, 1997, and November 12, 1997, and was aimed at studying the chemical effects of aircraft emissions in the North Atlantic flight corridor. The measurement platform was a DC-8 equipped with 16 scientific instruments. Below we briefly describe the instruments relevant for this paper: the meteorological measurement system (MMS), the differential absorption lidar (DIAL), the microwave temperature profiler (MTP), the in situ ozone probe, the differential absorption CO measurement (DACOM), and the laser hygrometer.

The MMS measured the air velocity with respect to the aircraft and the aircraft velocity with respect to the Earth and combined the two vectors to get the zonal u, meridional v, and vertical w wind components. The air motion system consisted of two 5-hole differential pressure probes (Rosemount 858Y), three total temperature probes with different response times, a pitot static pressure probe, and a dedicated static pressure system. The aircraft motion sensing system consisted of a high-resolution inertial navigation device (Litton LTN-72RH), an embedded GPS ring laser inertial navigation instrument (Litton LN-100G), and a multiple-antenna GPS attitude reference system (Trimble TANS Vector).

[1]Department of Earth, Atmospheric, and Planetary Sciences, Massachusetts Institute of Technology, Cambridge.
[2]NASA Ames Research Center, Moffett Field, California.
[3]NASA Langley Research Center, Hampton, Virginia.
[4]Science Applications International Corporation, Hampton, Virginia.
[5]NASA Jet Propulsion Laboratory, Pasadena, California.
[6]NASA Goddard Space Flight Center, Greenbelt, Maryland.

Copyright 1999 by the American Geophysical Union.

Paper number 1999JD900430.
0148-0227/99/1999JD900430$09.00

The data stream was sampled at 65 Hz, then subsequently reduced to 5 and 1 Hz for postmission analysis. Pressure p and temperature T were also obtained from these probes, and then potential temperature θ was calculated from those values. The turbulent energy dissipation rate ϵ was estimated from a frequency band of 0.8 to 1.5 Hz. For data accuracy, resolution, and the method for estimating ϵ, see *Chan et al.* [1998].

The DIAL system was used to remotely measure ozone and aerosols in the zenith and nadir directions. Two frequency-doubled Nd:YAG lasers were used to pump two frequency-doubled, tunable dye lasers. One of the dye lasers was operated at 292 nm for the DIAL on-line wavelength of ozone, and the other one was operated at 300 nm for the off-line wavelength. The output beams were transmitted out of the aircraft coaxially with the receiver telescopes. The backscattered laser energy was collected by two back-to-back 36-cm-diameter telescopes. The analog signals from the detectors were digitized at 5 MHz to a 12-bit accuracy, and the averaged digitized signals were stored every 2 s. The data sampling resolutions used in our study are 90 m in altitude and 60 s in time. An earlier version of this instrument made the first remote measurements of ozone and aerosols across a tropopause fold [*Browell et al.*, 1987]. More details on the system are available elsewhere [*Browell et al.*, 1998; W. B. Grant et al., Observations of tropical boundary layer air masses in the northern midlatitude upper troposphere during SONEX, submitted to the *Journal of Geophysical Research*, 1999].

The MTP, a passive microwave radiometer, measured the natural thermal emission from oxygen molecules at three frequencies (55.51, 56.66, and 58.79 GHz). It is viewed at 10 elevation angles between $-80°$ and $80°$ using a scanning mirror, yielding a vertical temperature profile from near the surface to 24 km for each 16-s cycle. The altitude resolution was thus variable, being best ($\sim$150 m) near the aircraft altitude, and degrading with distance from the aircraft. The postflight results were calibrated against 42 rawinsondes launched near the DC-8 flight track during the two transit flights between California and Maine. These provided an absolute accuracy of 0.5 K rms near the aircraft altitude; this degrades with distance, becoming $\ll$1.5 K rms 3 km away. See *Denning et al.* [1989] for further information.

Ozone was measured in situ with the $NO+O_3$ chemiluminescence principle [*Clough and Thrush*, 1967]. On the basis of the sample exchange rate at sea level the response time of the probe was estimated to be $\sim$1 s with faster response at higher altitudes. Samples were taken at 6 Hz then averaged to 1 Hz. The data were further corrected for water vapor quenching effects using the hygrometer measurements. The accuracy is estimated to be 5%, or 2 ppbv, and the precision is estimated to be 2%, or 0.8 ppbv.

The DACOM measured CO, N_2O, and CH_4 in situ with a folded path, tunable diode laser spectrometer using a differential absorption technique [*Sachse et al.*, 1987; *Collins et al.*, 1996]. Again, the response time was estimated to be $\sim$1 s based on the sample exchange rate. There were quasiperiodic gaps in the data of order 30 s every $\sim$10 min because of the real-time calibration procedure, which was necessary to account for slow drifts in instrument sensitivity.

The laser hygrometer consisted of a compact laser transceiver mounted to an aircraft window plus a sheet of retroreflecting "road sign" material affixed to an outboard engine enclosure to complete the optical loop. Using differential absorption techniques, H_2O was sensed along this external path to an estimated precision of 2% in mixing ratio with a response time of 50 ms. See S. Vay et al. (Tropospheric water vapor measurements over the North Atlantic during SONEX, submitted to the *Journal of Geophysical Research*, 1999) for further details.

3. Observations

After two test flights out of its home base at Moffett Field, California, the DC-8 flew cross-country to Bangor, Maine, on October 13, 1997. A prominent stratospheric intrusion was present over the northcentral plains, and the DC-8 traversed its south end (Plate 1). The section of the tropopause fold penetrated by the aircraft was downstream of a trough and on the west side of a jet at the aircraft level. Satellite images showed a clear column of air along the eastern flank of the intrusion bordered farther east by a line of storm clouds associated with an accompanying lower-level cold front. Details will be shown and discussed in section 3.1.

During the next flight on October 15, 1997, the DC-8 encountered another stratospheric intrusion over the mid-Atlantic as it flew from Bangor to Shannon, Ireland (Plate 2). This time the fold existed on both the upstream and downstream sides of the trough. The aircraft, flying at $\sim$3 km, passed through the lower tip of the western branch of the fold, then again traversed the same fold as it ascended steeply to over 7 km. It then entered the main body of the intrusion and ascended in steps as it crossed through to the eastern side. The vertical cross-sectional view will be shown and discussed in section 3.2.

Some of the subsequent flights during SONEX also sampled stratospheric intrusions, but we will focus our analysis on these two events because only in these cases did the aircraft ascend (or descend) through a tropopause fold giving us vertical profiles of data necessary for estimating high-resolution gradient and flux quantities.

3.1. Case 1: October 13, 1997

Plate 3 is a "curtain plot" of ozone concentration measured by the DIAL as the DC-8 flew under then up through the tropopause fold. The DC-8 was flying at a fairly constant air speed of $\sim$220 m s^{-1} (the

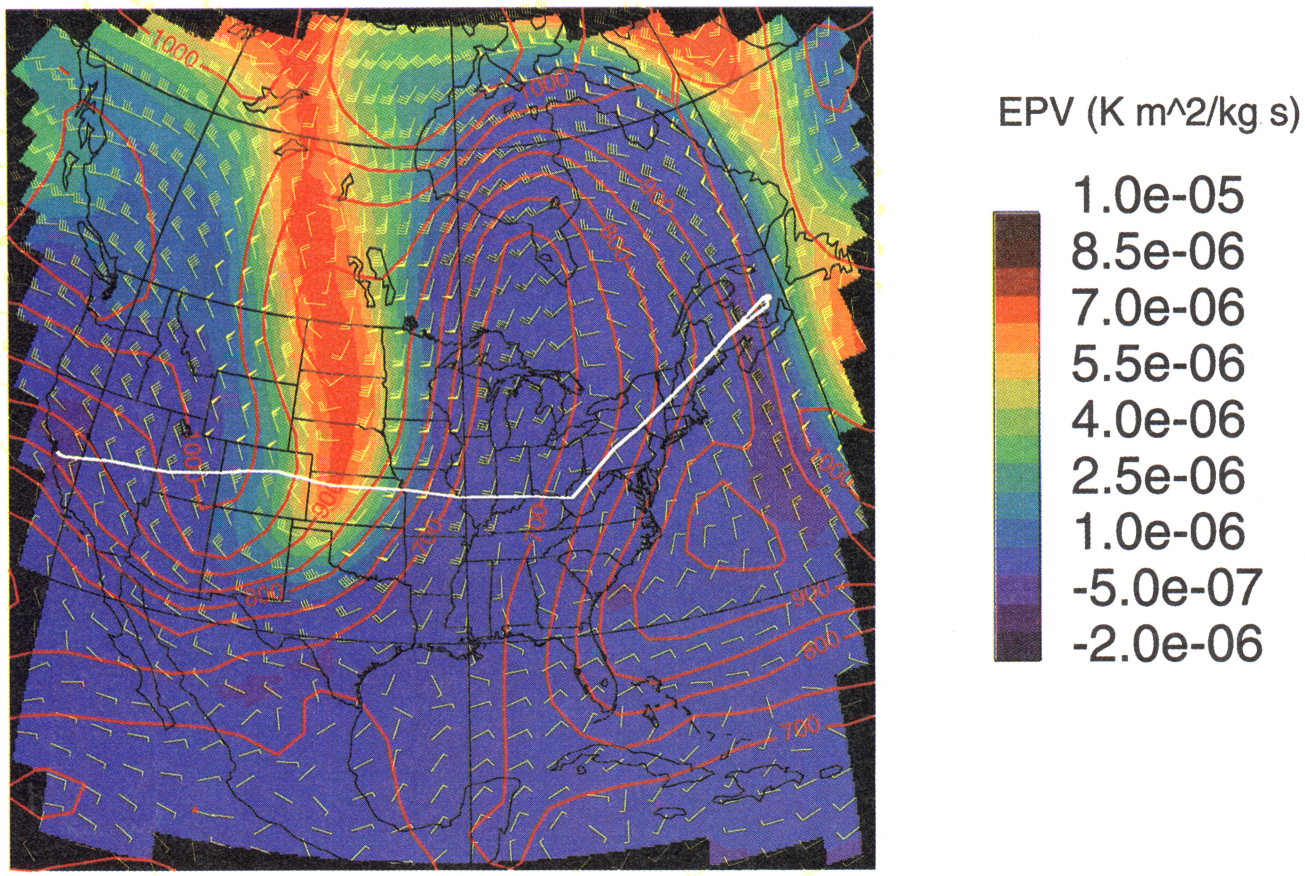

Plate 1. Map of geopotential height in decameters (red contour lines), Ertel's potential vorticity (color scale), and horizontal winds (yellow vectors) on the 330-K surface for 1200 UT, October 13, 1997. The scaling on the wind vectors is standard: one flag is 50 m s^{-1}, one bar is 10 m s^{-1}, and one half bar is 5 m s^{-1}. The plotted field values were output from a model run by the Data Assimilation Office of the NASA Goddard Space Flight Center (A. M. Thompson et al., The Goddard/Ames meteorological support and modeling system during SONEX: Evaluation of analyses and trajectory-based model products, submitted to the *Journal of Geophysical Research*, 1999). The longitudinal and latitudinal grid spacing used by the model was 2.5° by 2°. The white line shows the flight path of the DC-8, which departed Moffett Field, California, at 1519 UT and landed in Bangor, Maine, at 2241 UT.

ground speed was slightly higher), so roughly 1 hour corresponds to ~800 km. Because of the incomplete overlap of the transmitted beam and the receiver field of view at close range, there were no data from the DIAL in the height range delineated by the dashed lines. In this region the data were linearly interpolated by also including the in situ measurement of ozone at the aircraft level, hence the vertical blurring of the image in this zone. The apparent widening of the fold where the aircraft cut across it was probably not real.

In situ measurements of trace gases reveal the fine structure present within the fold (Figure 1). The detailed anticorrelation of O_3 versus CO, N_2O, and H_2O shows the intermingling of stratospheric and tropospheric air. (The CH_4 trace, not shown here, was virtually identical to that of CO.) Within what appeared to be the main body of the fold from ~18.04 (1802:24) to ~18.09 (1805:24) UT the gradient in the ozone concentration was mainly in the vertical (upward) direction. (Whenever the time is given in decimal hour notation we will also give it in standard notation in parentheses. All figures and plates with time axes are labeled in decimal hours UT.) We deduce this from the observation that ozone remained steady as the aircraft was at level flight in the first half, while it increased as the aircraft ascended, and also from the positive correlation between small-scale fluctuations of ozone and potential temperature in Figure 2. Just after 18.06 (1803:36) UT when the aircraft began to ascend, there was a rapid oscillation in the trace constituent concentrations. We will argue in section 3.1.1 that this was a manifestation of a Kelvin-Helmholtz instability.

As the aircraft continued to climb, there was a secondary maximum in the ozone measurement (and minima in the other shown constituents) just after 18.11 (1806:36) UT. A possible third local maximum in ozone began ~18.14 (1808:24) UT. The sharp edge on the topside of the main fold and this secondary maxima

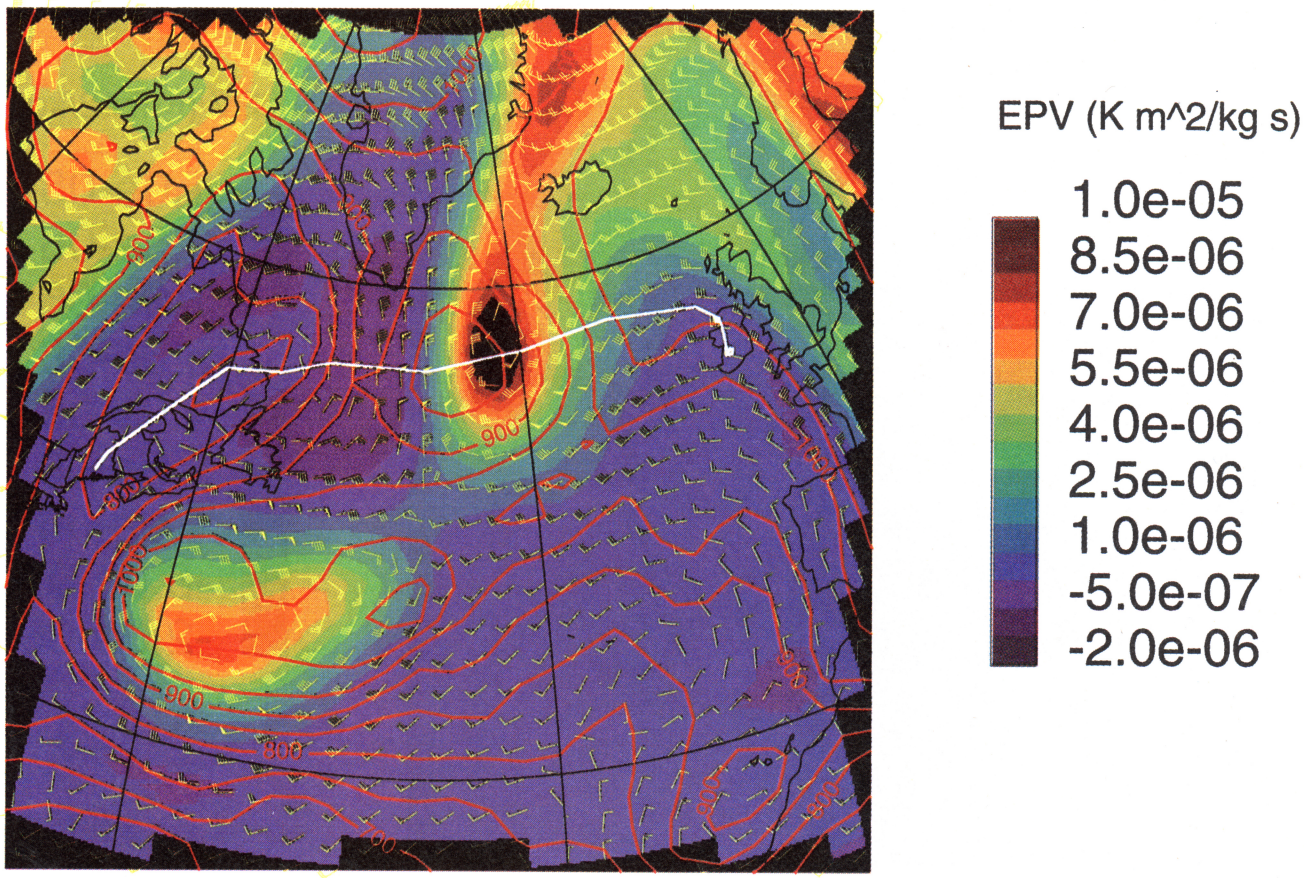

Plate 2. Same as Plate 1, except for October 15, 1997. The DC-8 departed Bangor at 1211 UT and landed in Shannon, Ireland, at 1821 UT.

are reminiscent of past in situ observations [*Danielsen et al.*, 1970; *Shapiro*, 1974; *Danielsen and Mohnen*, 1977; *Johnson and Viezee*, 1981]. Unfortunately, the resolution and the near-field blind zone of the DIAL did not allow us to observe the two-dimensional character of these substructures.

The dynamical measurements are displayed in Figure 3. The increase in horizontal wind speed, especially in the meridional, as the aircraft ascended through then away from the fold is consistent with the classic picture of the jet stationed above the topside of the tropopause fold, inducing the secondary circulation necessary for folding. Clearly, the background wind shear was quite strong in this region beneath the jet. The rapid oscillation seen just after 18.06 (1803:36) UT in the tracers are also visible here, especially in θ and u. Turbulence, as indicated by $\log \epsilon$, peaked at the edge of the main fold's topside (18.09 (1805:24) UT), around the second ozone maximum (~18.12 (1807:12) UT), and at the beginning of the third ozone maximum (just before 18.14 (1808:24) UT). There appears to be some correlation between ϵ, relative upward motion, and a decrease in $d\theta/dz$, which is suggestive of convective instability.

3.1.1. Dynamical (Kelvin-Helmholtz) instability. Let us now look closer at the rapid oscillations observed in both chemical and meteorological quantities shortly after 18.06 (1803:36) UT. Figure 2 shows the periodic undulations in tracer and dynamical measurements suggestive of Kelvin-Helmholtz (KH) billows. The perturbations in v were much smaller than in u, which is consistent with the plane of the vertical shear (estimated from the data to be 59°, measured clockwise from the north) being in closer alignment in the zonal direction than in the meridional direction.

Assuming that the oscillations were, indeed, KH billows, we can estimate their horizontal wavelength and vertical thickness. Along the aircraft heading the period was ~5.5 s, which translates to a length of 1.23 km at the aircraft speed of 224 m s^{-1}. Since the aircraft heading was 102°, this yields a true horizontal wavelength of $\lambda_h = 1230 \cos(102° - 59°) = 900$ m. The vertical thickness is then given by the relationship $\Delta z = \lambda_h/7.5 = 120$ m [*Miles and Howard*, 1964]. These numbers are quite similar to those of rapid oscillations observed near the tropopause by a uniquely high-resolution radar experiment [*Cho et al.*, 1996].

However, the calculated gradient Richardson number for the height interval across the presumed KH layer is $Ri = 0.52$, which is larger than the classic instability criterion of 0.25. It could be that the aircraft was al-

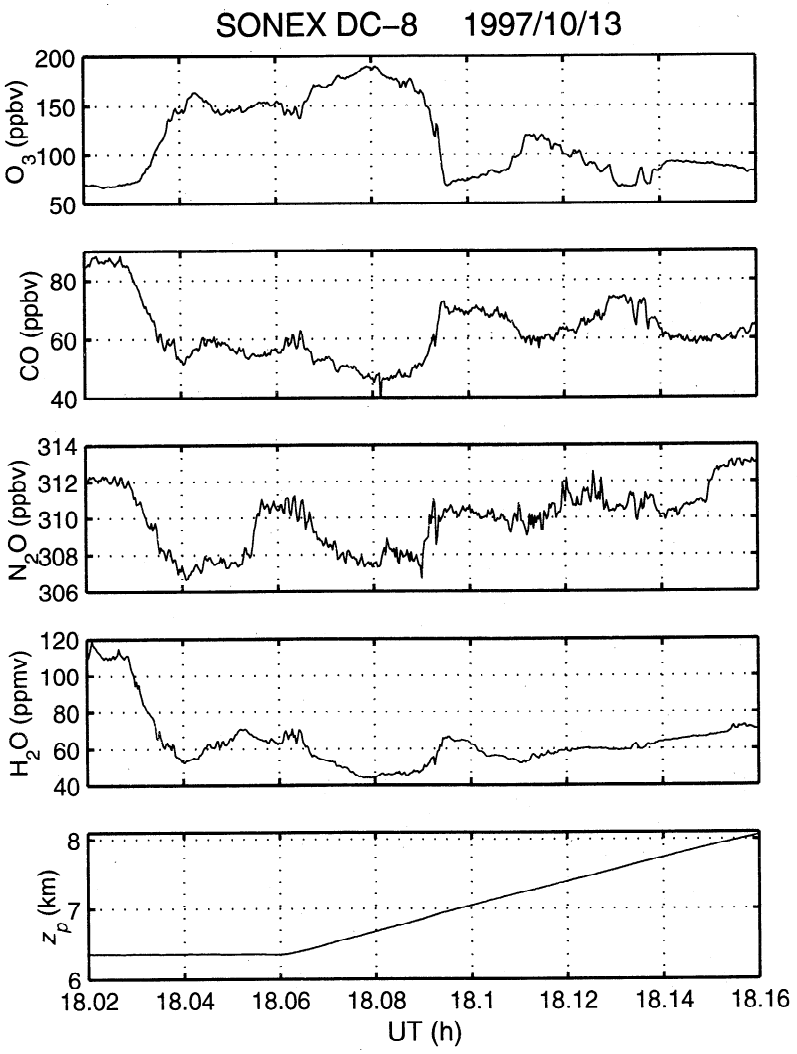

Figure 1. Plots, from top to bottom, of O_3, CO, N_2O, and H_2O mixing ratios through the tropopause fold region on October 13, 1997, and the pressure altitude of the aircraft.

ready within the instability layer as it began its ascent, since the oscillation in the data began just as the climb began. If this were true, then the extra wind shear necessary to bring Ri down to 0.25 may have existed just below the aircraft height at 18.06 (1803:36) UT. Also, the instability may have been in a decay phase where Ri could be larger than 0.25. Finally, because the aircraft flew more horizontally than vertically, horizontal gradients could have mapped into the estimated vertical gradients and caused them to be underestimated.

Because the apparent KH instability occurred in the middle of the tropopause fold, it would not have been effective in mixing the air inside the fold with the air outside. Mainly, it would have smoothed the vertical gradients of quantities within the instability layer. In terms of stratosphere-troposphere exchange we are more interested in turbulence occurring at the edge of the fold and also around the secondary maxima observed in ozone just outside the main fold region.

3.1.2. Convective (Rayleigh-Taylor) instability. We now turn our attention to the topside of the tropopause fold and to the secondary maxima in ozone that followed shortly. The bottomside of the fold was not associated with any appreciable turbulence, so we will not discuss it here.

Figure 4 shows the changes in the squares of the Brunt-Väisälä frequency N and vertical shear in horizontal winds dU/dz as well as the resulting Ri. For ease of comparison, we display $\log \epsilon$, w, and ozone concentration below them. To calculate the vertical gradients, we fit a straight line in a least squares sense to the quantity versus altitude for an interval ± 60 m from the data point. This 120 m represents the outer scale of turbulence L_0, which varies according to $L_0 = (2\pi/0.62)\epsilon^{1/2}N^{-3/2}$ [*Weinstock*, 1978]. We get $L_0 = 120$ m if we take $\epsilon = 4 \times 10^{-4}$ W kg^{-1} (the high value measured by the MMS in this vicinity) and $N^2 = 2 \times 10^{-4}$ rad^2 s^{-2} (a typical value calculated from MTP

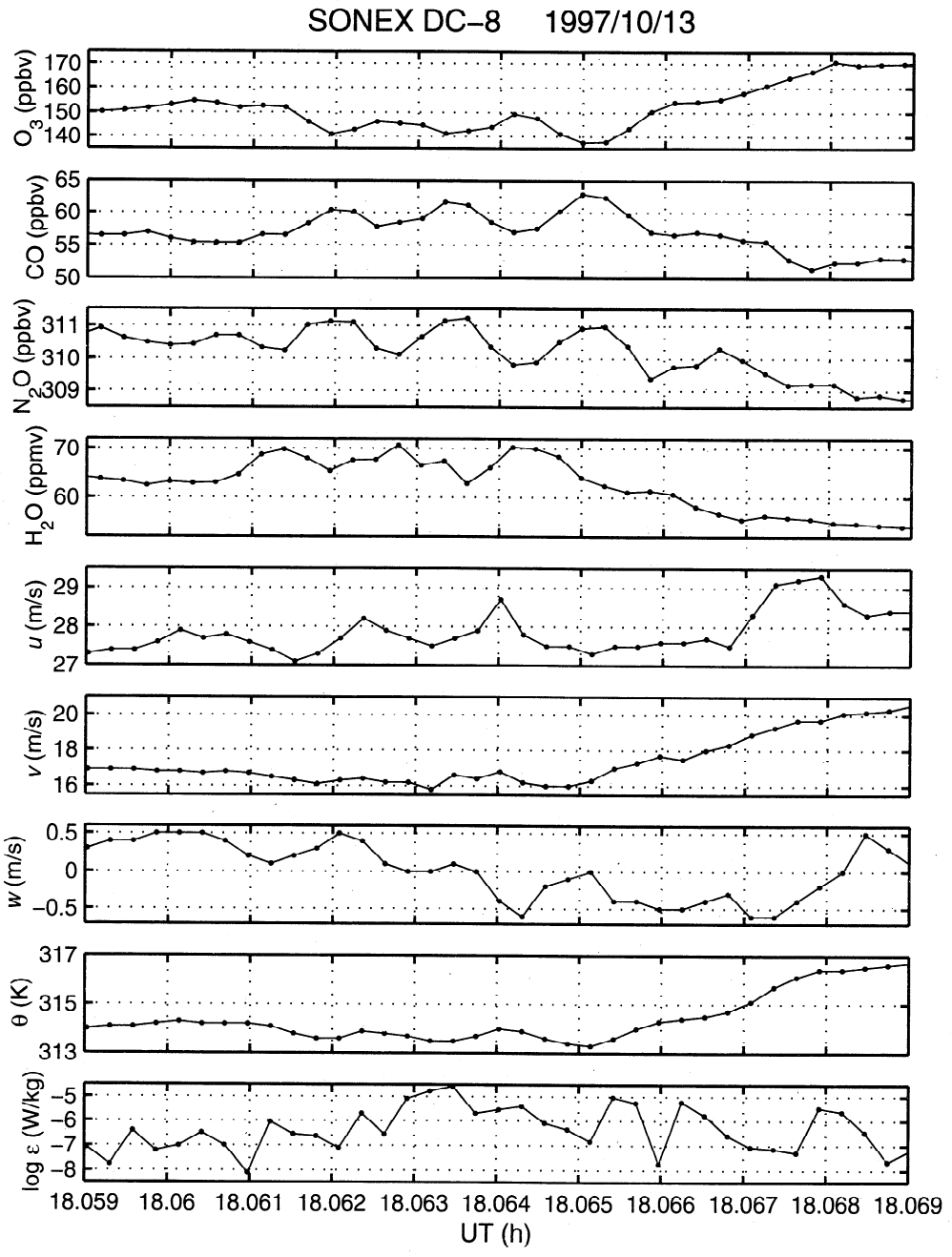

Figure 2. Expanded time plots, from top to bottom, of O_3, CO, N_2O, H_2O, the zonal wind component u, meridional wind component v, vertical wind component w, potential temperature θ, and turbulence $\log \epsilon$ from October 13, 1997.

profiles). Also, the observation of a nearby dynamically unstable layer of the same thickness indicates that this is a reasonable value.

For regions with $Ri < 0.25$, there was a clear correspondence between high thermal stability N^2 and high vertical shear. This preference for dynamic instability to occur across layers of enhanced thermal stability is in keeping with both theory [*Phillips*, 1966] and past observations [e.g., *Fritts and Rastogi*, 1985]. There was also a convectively unstable period between ~18.116 (1806:58) and ~18.124 (1807:26) UT when N^2 and Ri became negative. Note that the vertical shear was very low during this time, which is consistent with the convective instability of high-frequency gravity waves in both theory and laboratory observations [*Orlanski*, 1972]. The same region experienced strong turbulence and large perturbations in upward velocity, which also points to convective instability. Furthermore, the gravity wave breakdown interpretation is supported by a wavelike perturbation in u, v, and θ with maxima in

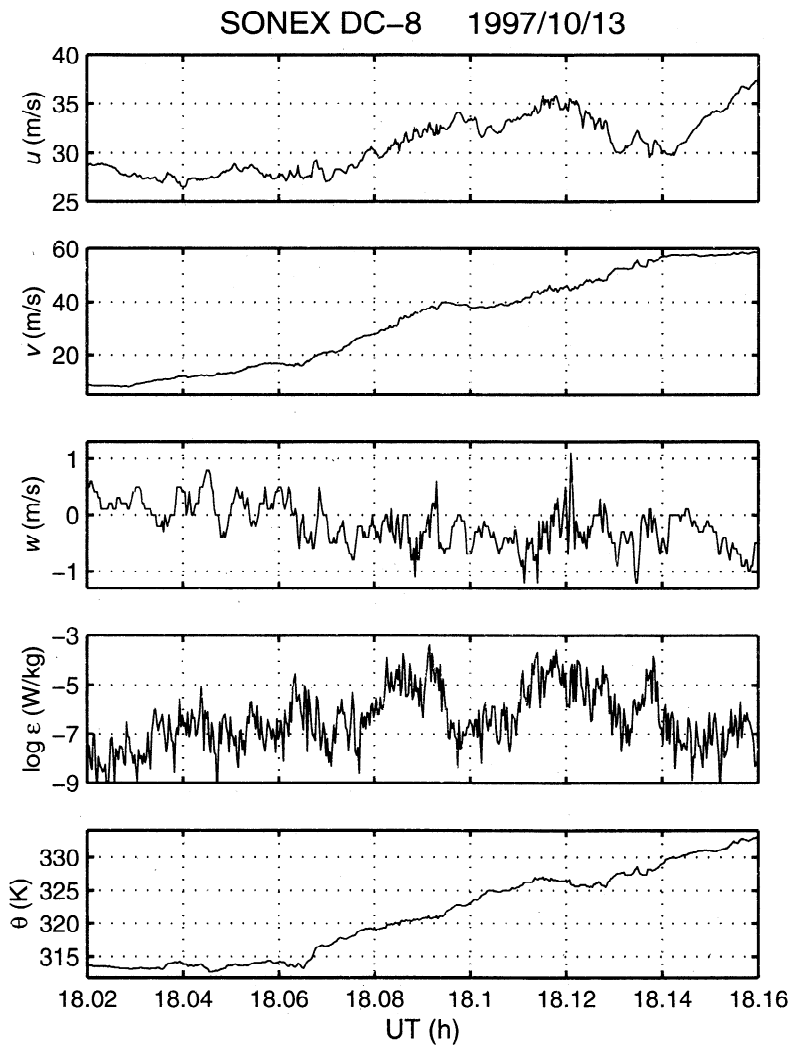

Figure 3. Plots, from top to bottom, of u, v, w, $\log\epsilon$, and θ through the tropopause fold region on October 13, 1997.

the wind components and minima in $d\theta/dz$ at ~18.09 (1805:24) and ~18.12 (1807:12) UT. Even the enhancements in fine-scale u and v perturbations at the "crests" are suggestive of wave breakdown. Although N^2 did not become negative ~18.09 (1805:24) UT, it did reach a local minimum. If the gravity wave breakdown explanation is correct, then the secondary ozone maximum ~18.12 (1807:12) UT was probably the result of either vertical wave advection of the tropopause fold or upward, irreversible turbulent mixing of ozone or both.

Of course, vertical gradient quantities calculated from a slantwise flight are only approximations. Remotely sensed data from the MTP did not indicate a superadiabatic lapse rate ~18.12 (1807:12) UT, but the instrument only gave a reading every 16 s with a vertical resolution of about ~150 m, so it could have missed a localized instability. To examine the situation in two dimensions, we can draw upon past numerical models of convectively breaking gravity waves. Figure 5 is a sequential schematic of three potential temperature isopleths perturbed by a gravity wave until convective overturning occurs. The heavy lines indicate the hypothetical paths of an ascending aircraft and potential temperature increases with height as indicated. Note that $d\theta/dl$, the gradient along the aircraft path, only becomes negative as the isopleths tilt more steeply than the aircraft ascent angle. Although only a qualitative sketch, an important feature illustrated here that is seen in models is the stretching of the isentrope spacing in the horizontal direction as the wave grows [e.g., *Walterscheid and Schubert*, 1990]. Typically, as the overturning begins, the potential temperature horizontal gradient is an order of magnitude less than the background vertical gradient. If the aircraft could as-

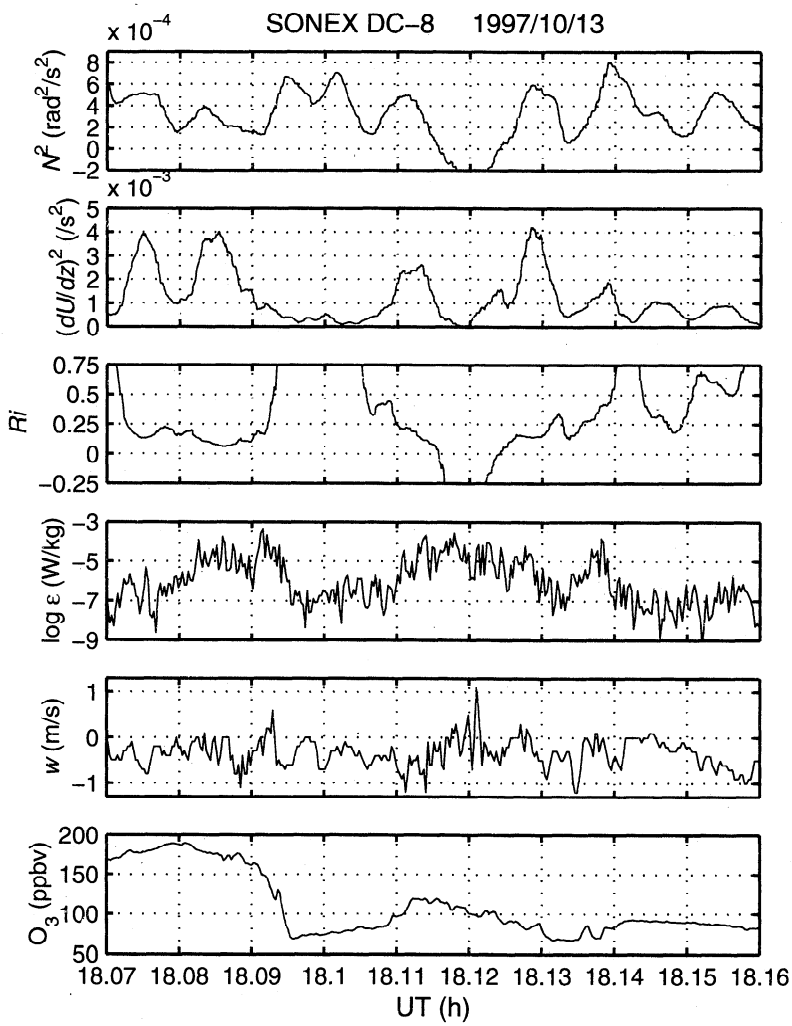

Figure 4. Plots, from top to bottom, of the Brunt-Väisälä frequency squared N^2, vertical shear squared $(dU/dz)^2$, Richardson number Ri, $\log \epsilon$, w, and O_3 mixing ratio from October 13, 1997.

cend purely vertically, then convective instability would be detected as $d\theta/dl = d\theta/dz \leq 0$; however, since it was moving mostly horizontally in this case (at a slope of ~1:50), if the magnitude of $d\theta/dl$ was more than, say, one tenth of the background vertical gradient, then there would be strong evidence for convective instability. Around 18.12 (1807:12) UT we estimate the background potential temperature vertical gradient to have been ~0.007 K m^{-1} from the MTP, while MMS data showed that $|d\theta/dl|$ (negative gradient) reached as high as 0.003 K m^{-1}, thus supporting the conclusion that there was an area of convective instability there.

3.1.3. Tropopause fold turbulent ozone flux. We can now estimate the vertical tracer flux from the tropopause fold to the ambient troposphere induced by turbulence generated by convective and dynamical instabilities. We will use ozone as the example tracer.

For a stably stratified ($N^2 > 0$) environment we apply the vertical eddy diffusivity

$$K_z = \alpha \frac{\epsilon}{N^2} , \quad (1)$$

where α is a proportionality factor that varies with the flow conditions [e.g., *Itsweire et al.*, 1986]. We invoke the expression derived by *Weinstock* [1992]

$$\alpha = 0.6 \left(\frac{L_e}{L_b}\right)^{\frac{4}{3}} e^{-0.51\left(\frac{L_\nu}{L_e}\right)^{\frac{4}{3}}} , \quad (2)$$

where $L_e = -2(2)^{1/2}\rho'(\partial\rho/\partial z)^{-1}$ is the vertical energy-containing scale of turbulence with ρ' the rms air density fluctuation and ρ the background air density, $L_b = 2\pi\epsilon^{1/2}N^{-3/2}$ is the buoyancy scale, and $L_\nu = 31\nu^{3/4}\epsilon^{-1/4}$ is the viscous dissipation scale with kinematic viscosity $\nu = 1.458 \times 10^{-6}T^{3/2}/[(T + 110.4)\rho]$ (Sutherland's formula). Here ρ can be calculated from p and T through the ideal gas law $p = \rho RT$, where R is the gas constant for air.

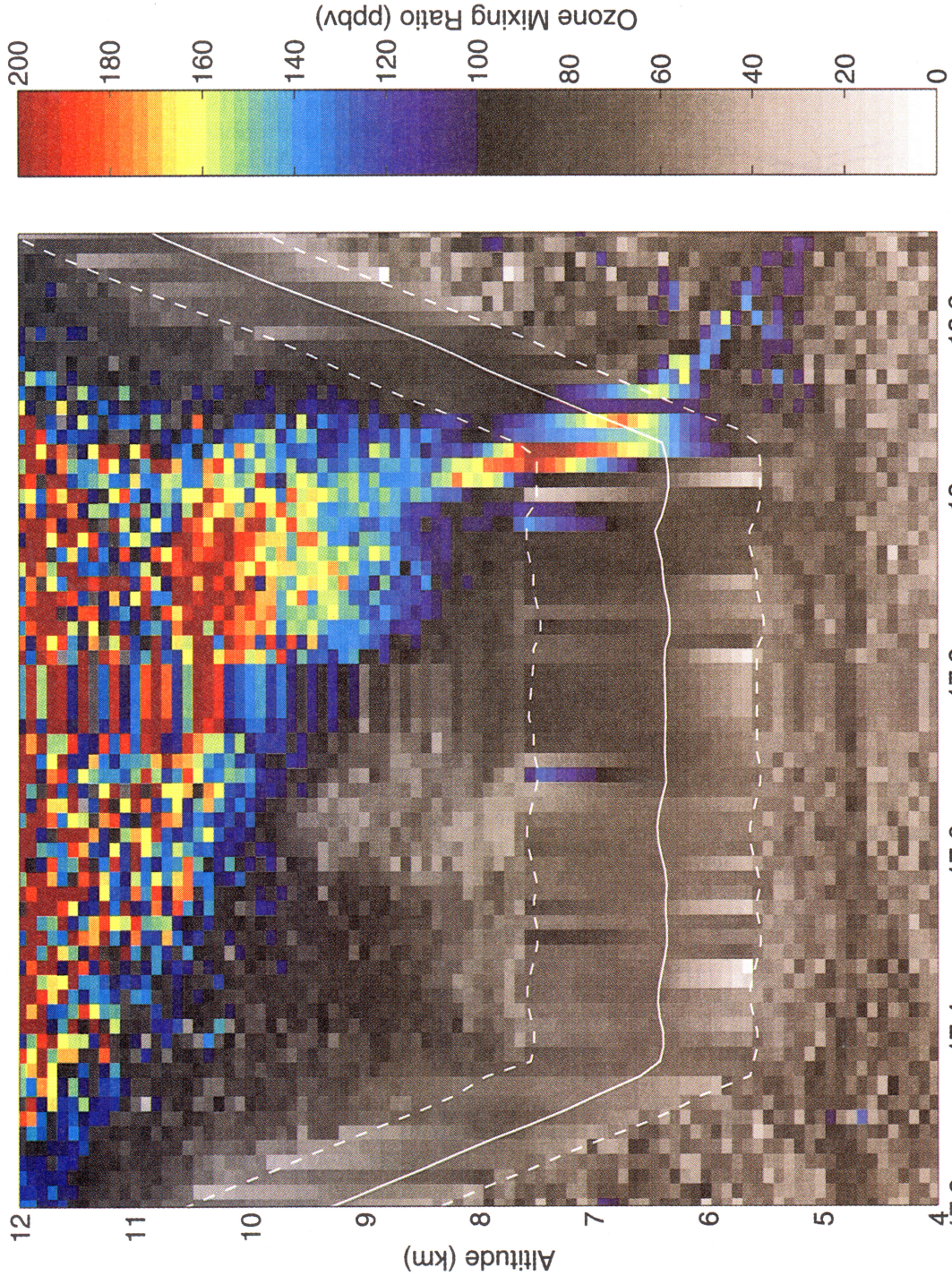

Plate 3. DIAL ozone measurements made in the vicinity of the tropopause fold over the central United States on October 13, 1997. The white solid line shows the altitude of the aircraft, and the dashed white lines demarcate the zone of no data. In this region the data were linearly interpolated over altitude including also the in situ ozone measurement at aircraft level. There were also missing data between 17.7 (1742:00) UT and 17.8 (1748:00) UT. (Whenever the time in the text is given in decimal hour notation we will also give it in standard notation in parentheses. All figures and plates with time axes are labeled in decimal hours UT.) The position of the aircraft was 39.6°N, 103.3°W at the beginning of the plot and was 39.0°N, 92.0°W at the end of the plot. Its heading during this interval was generally westward, varying between 70° and 114°.

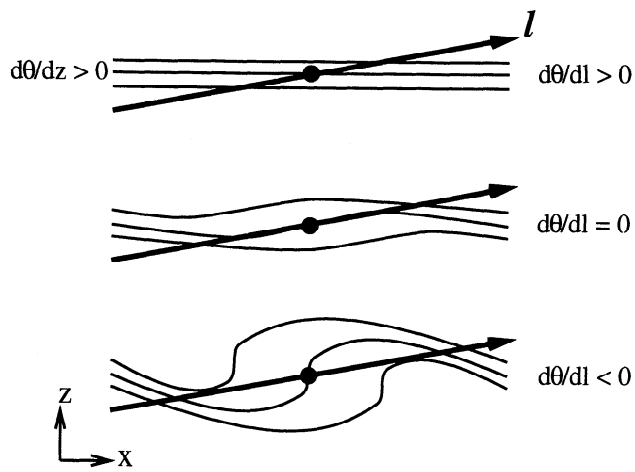

Figure 5. Sequential schematic of three potential temperature isopleths perturbed by a gravity wave until convective overturning occurs. The heavy lines represent the hypothetical paths of an ascending aircraft. The length variable along these paths is l, and z is upward and x is horizontal. The $d\theta/dl$ values are for the center dot area.

For unstable and neutral conditions ($N^2 \leq 0$), we use

$$K_z = \beta \left(\frac{g\,|\Delta\theta|\,K_m^2}{\theta\nu} \right)^{\frac{1}{3}} \Delta z\ , \qquad (3)$$

where β is an empirical constant, g is the gravitational acceleration, $\Delta\theta$ and Δz are the vertical temperature difference and thickness across the unstable region, and K_m is the molecular diffusivity [*Kraichnan*, 1962; *Orlanski and Ross*, 1973]. We choose $\beta = 0.08$, following the laboratory results of *Ingersoll* [1966]. Using the relation $K_m/\nu = 1.34$ [*Chapman and Cowling*, 1970], Sutherland's formula, and the ideal gas law, (3) becomes

$$K_z = 1.57 \times 10^{-3} \left[\frac{g\,|\Delta\theta|}{\theta\,(T + 110.4)\,p} \right]^{\frac{1}{3}} T^{\frac{5}{6}} \Delta z\ , \qquad (4)$$

where p is in hPa. The vertical flux of trace constituent mixing ratio χ is then given by

$$\Phi_\chi = -K_z \frac{d\chi}{dz}\ . \qquad (5)$$

Figure 6 shows the resulting K_z and Φ_{O_3} calculated for the same period as covered by Figure 4. The ozone mixing ratio and its vertical gradient are also plotted for reference. The background gradient quantities were calculated in the same way as for Figure 4. Between ~18.115 (1806:54) and ~18.125 (1807:30) UT when N^2 was ≤ 0, we took $|\Delta\theta| = 1.5$ K and $\Delta z = 225$ m for (4). K_z is relatively constant in this region because the T and p fluctuations in (4) were much smaller than the ϵ fluctuations in (1). Although it may be counterintuitive that convective instability would not yield a much larger K_z, the reduction of the local vertical gradient by the breaking wave limits the turbulent vertical constituent flux [*Fritts and Dunkerton*, 1985]. The largest ozone flux is upward from the topside of the "main" body of the tropopause fold, which is interesting since one usually thinks of stratosphere-to-troposphere transfer in terms of downward flux. The values are in excellent agreement with those estimated by *Shapiro* [1980] ($\Phi_{O_3} = 1.3$–1.4 m s^{-1} ppbv on the topside of folds), which is remarkable considering that we used a completely different estimation method. The average value of $K_z = 4.4$ m^2 s^{-1} calculated by *Danielsen et al.* [1987] from a simple three-dimensional model of a tropopause fold is somewhat larger than our values but not very different considering the variability of the fold structure. We did not calculate Φ_{O_3} for the bottomside of the fold because the aircraft was flying level there and we could not estimate the vertical gradient quantities. However, as seen in Figures 1 and 3, the turbulence was very much weaker on the bottomside, so we believe the vertical mixing there was negligible.

We must, however, insert a cautionary note regarding our estimates of K_z and Φ_{O_3}. First, as mentioned before, horizontal gradients may be mapped into vertical gradients estimated from slant path data. Although K_z is dominated by ϵ variations, Φ_{O_3} is linearly proportional to the vertical ozone gradient. Thus the vertical ozone gradient is a crucial quantity, especially its sign. The "vertical" structure of the tropopause fold up to 18.1 (1806:00) UT matches nicely with the DIAL ozone data above and below. In fact, a comparison with Φ_{O_3} calculated with the interpolated DIAL ozone profiles supports the negative ozone gradient (and upward flux) just after 18.09 (1805:24) UT. However, the upward gradients (and downward fluxes) ~18.11 (1806:36) and ~18.14 (1808:24) UT are not observed in the DIAL-derived results. The associated ozone features were too small scale and local to show up in the DIAL data, and therefore we cannot confirm that the vertical gradient features there were not mainly produced by horizontal structures.

Second, (3) is not the only eddy diffusion formulation proposed for convective turbulence. For example, $K_z \sim |N|$ has also been suggested [*Priestley*, 1954; *Lilly*, 1962], which yields much higher K_z values for our two cases, so there is considerable uncertainty in eddy diffusivity under convective turbulence. However, there are theoretical reasons and experimental evidence favoring (3) [*Globe and Dropkin*, 1959; *Kraichnan*, 1962; *Ingersoll*, 1966]. Third, the method of estimating ϵ from 5-Hz dynamical measurements as outlined by *Chan et al.* [1998] has not been fully verified

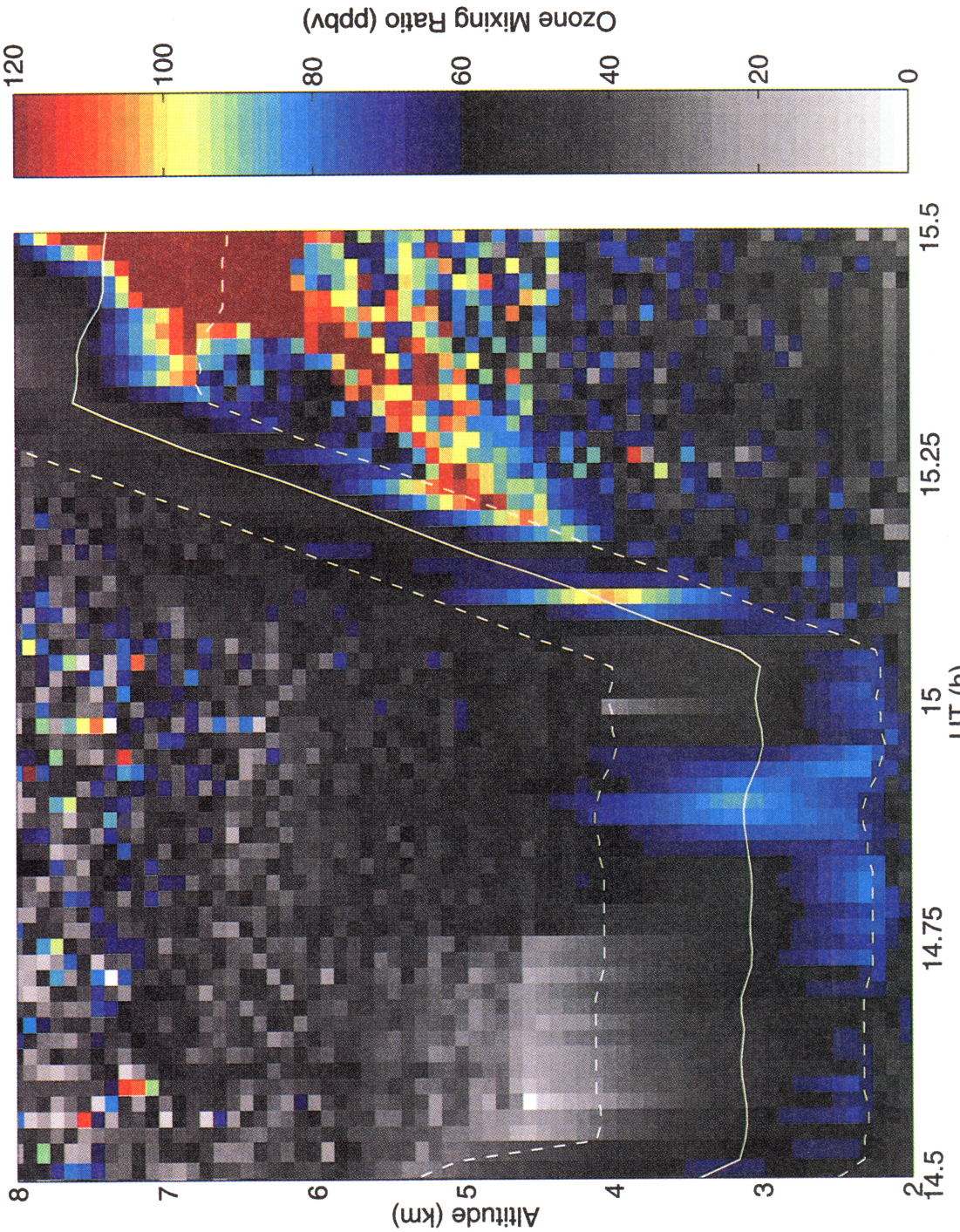

Plate 4. DIAL ozone measurements made in the vicinity of the western branch of the tropopause fold over the North Atlantic on October 15, 1997. The white solid line shows the altitude of the aircraft, and the dashed white lines demarcate the zone of no data. In this region the data were linearly interpolated over altitude including also the in situ ozone measurement at aircraft level. The position of the aircraft was 55.0°N, 48.7°W at the beginning of the plot and was 55.4°N, 36.8°W at the end of the plot. Its heading during this interval was generally westward, varying between 56° and 86°.

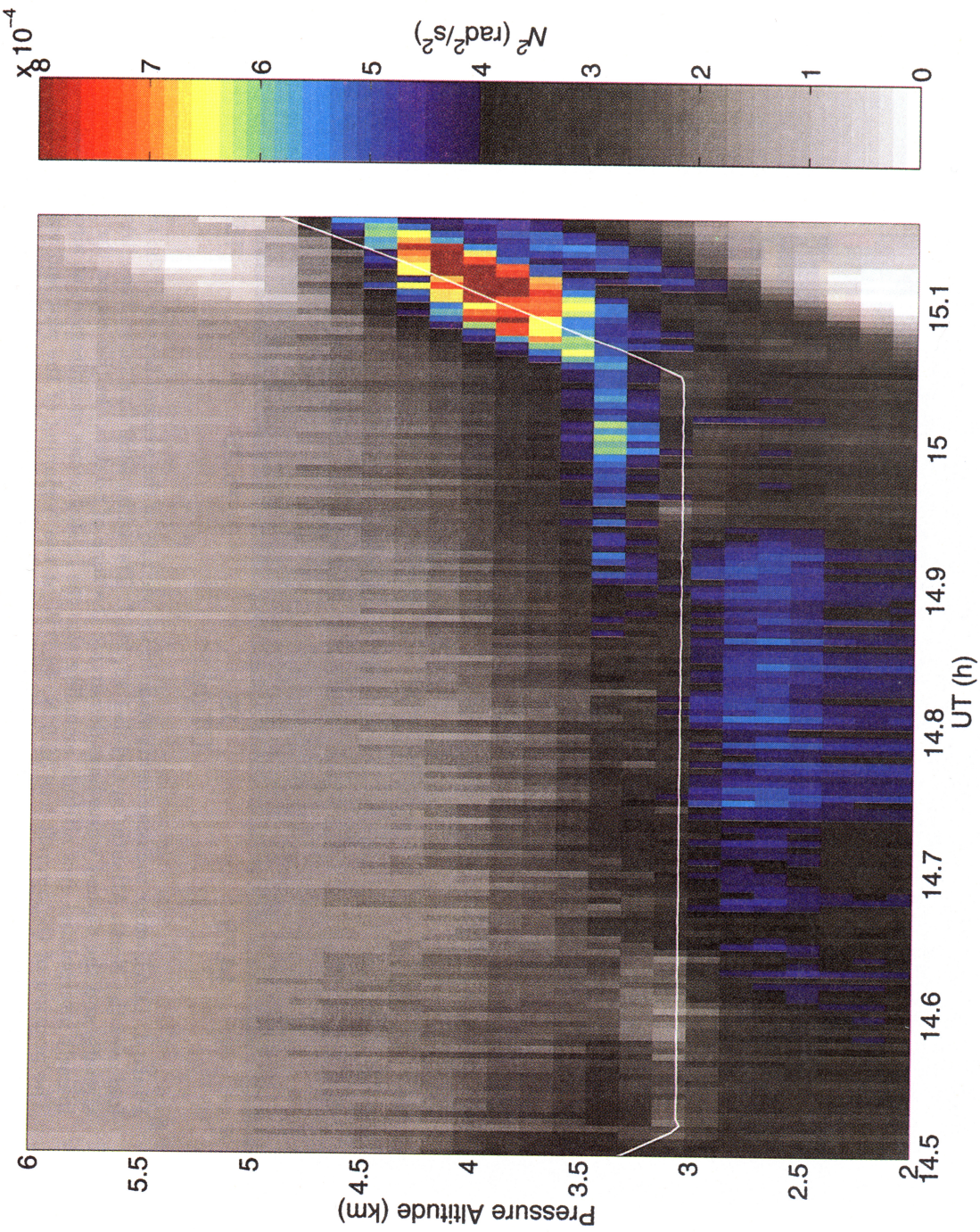

Plate 5. Vertical profiles of N^2 calculated from the MTP temperature data on October 15, 1997. The aircraft flight level is indicated by the white solid line.

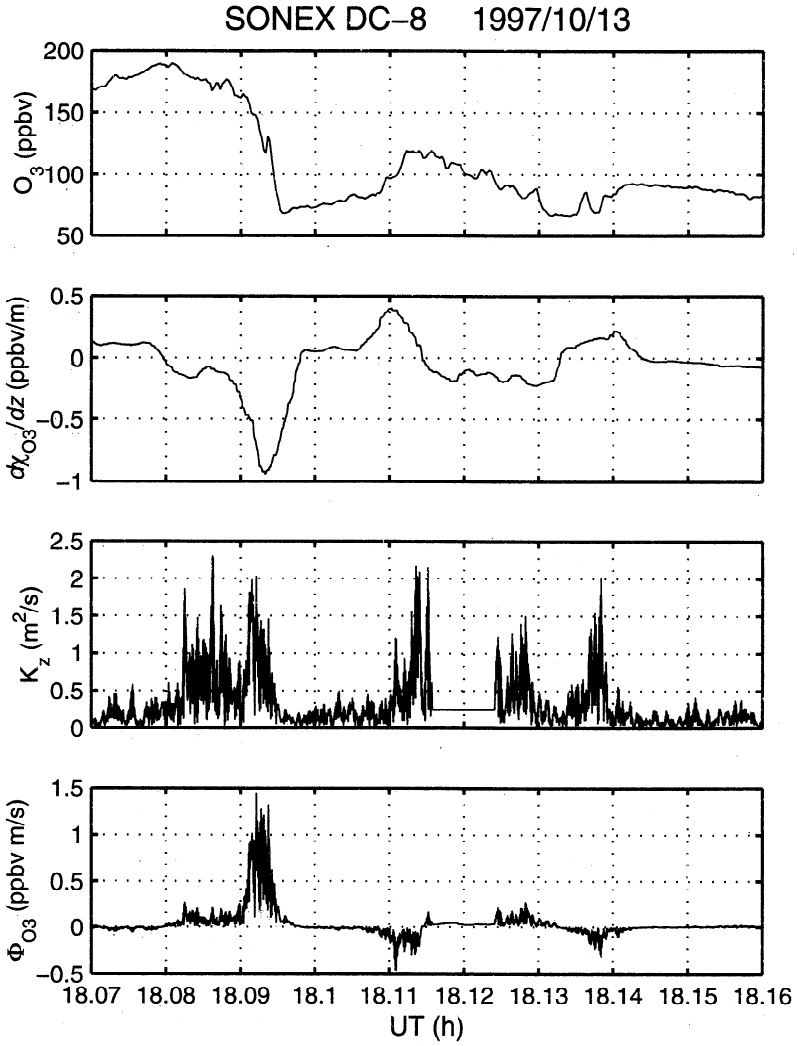

Figure 6. Plots, from top to bottom, of O_3 mixing ratio, vertical gradient of O_3 mixing ratio, vertical eddy diffusivity K_z, and vertical flux of O_3 mixing ratio from October 13, 1997.

by comparison with other instruments. We decided to use the K_z approach because the 1-s resolution of the tracer measurements was not fine enough for a direct eddy correlation ($\overline{w'\chi'}$, where the primed quantities are perturbations from the means) approach. In 1 s the aircraft traverses over 200 m, so the Nyquist length scale would be greater than the turbulent eddy scale, so $\overline{w'\chi'}$ would not represent turbulent flux, which is what we wanted in our investigation of irreversible transport.

3.2. Case 2: October 15, 1997

Plate 4 shows in color-scale form the vertical profiles of ozone concentration measured by the DIAL as the aircraft encountered the western branch of the tropopause fold (see also Plate 2). The apparent discontinuity in the fold was caused by the DIAL's near-field blind zone, marked by dashed lines in Plate 4. Thus the fold was not visible inside the blind zone except where the aircraft intersected it with the in situ probe. Following this "connect-the-dots" mental picture of the fold, one can see that the aircraft crossed it horizontally from topside to bottomside ~14.9 (1454:00) UT, then ascended through it from bottomside to topside ~15.1 (1506:00) UT. This scenario is supported by the plot of stability as characterized by N^2 calculated from the MTP temperature profiles (Plate 5). Although instrumental problems cut off the data at 15.16 (1509:36) UT, we can still see the layer of very stable stratospheric air extending down from the right-hand edge of the plot, leftward across the flight line ~15.1 (1506:00) UT, then down again through the flight path ~14.9 (1454:00) UT.

Figure 7 again shows the anticorrelation of O_3 versus CO and CH_4, clearly indicating the encounter with a lower portion (height ~3 km) of the tropopause fold at ~14.9 (1454:00) UT and a higher section (height ~4 km) at 15.1 (1506:00) UT. The aircraft began entering the main body of the stratospheric intrusion ~15.4 (1524:00) UT. We note the similarity of the upper part of the fold to case 1 in that the sharply defined topside was followed by a couple of weaker perturbations.

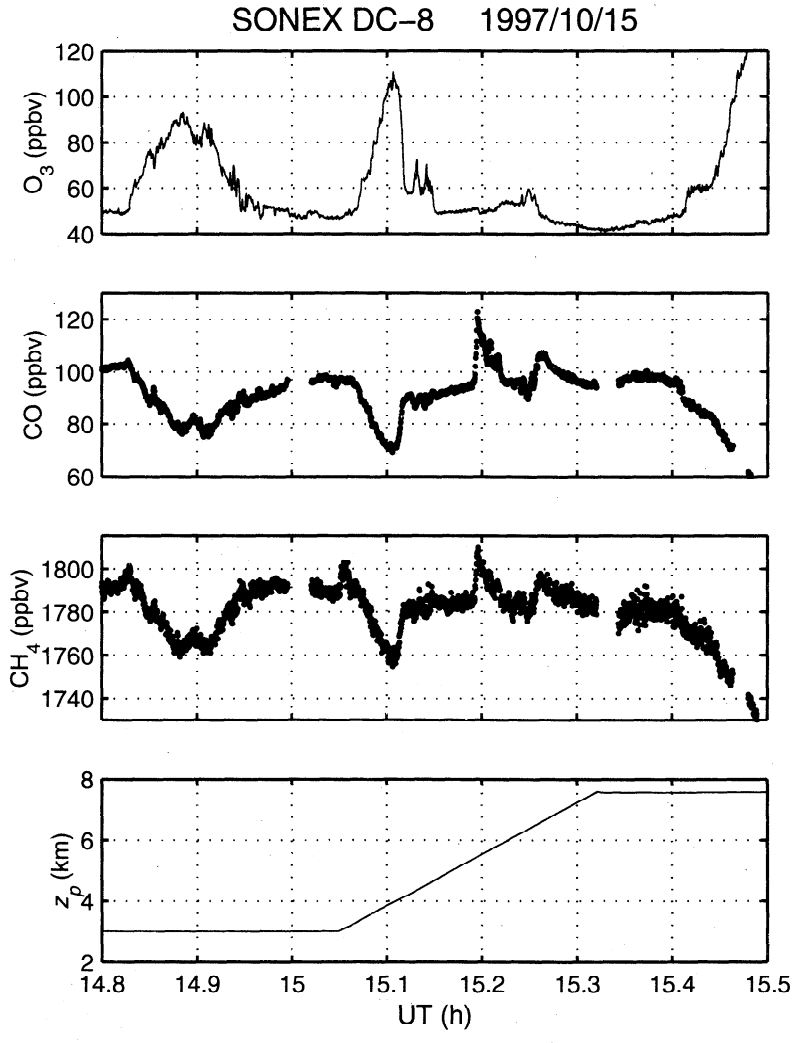

Figure 7. Plots, from top to bottom, of O_3, CO, and CH_4 mixing ratios through the two intersections with the western branch of the tropopause fold region on October 15, 1997, and the pressure altitude of the aircraft.

There was also a hint of a wavelike structure in the ozone trace on the the more diffuse bottomside. Fortunately, the aircraft was ascending through this region, so we will be able to estimate the vertical gradient quantities needed for instability analyses as we did for case 1.

The corresponding dynamical measurements are displayed in Figure 8. In the ascent region of interest (15.05–15.3 (1503:00–1518:00) UT), there was a zone of strong vertical shear and regular oscillations in w ~15.1 (1506:00) UT (more easily seen in Figure 9) corresponding to the second fold encounter. Together with the wavy bottomside seen in ozone, this suggests the presence of KH billows. Immediately following the shear zone was a fast oscillation with period ~0.01 hours in u that grew quickly with height and/or horizontal distance and appeared to break ~15.14 (1508:24) UT corresponding to a maximum in ϵ and to the secondary ozone maxima. This oscillation is marked by a horizontal bar with vertical tick marks separated by 0.01 hours above the u trace in Figure 8. This combination of dynamical and tracer observations was also seen in case 1, which we interpreted to be convectively breaking gravity waves. In this case the small-scale wave was superimposed on a larger-scale wave with period ~0.1 hours that also grew in amplitude with height and/or horizontal distance and appeared to break ~15.3–15.4 (1518:00–1524:00) UT. (This oscillation is marked by a horizontal bar with vertical tick marks separated by 0.1 hours below the u trace in Figure 8.) Note the strong enhancement in ϵ ~15.3–15.4 (1518:00–1524:00) UT. One can also see that $d\theta/dz$ was close to zero in the areas of suspected convective wave breaking. With one-dimensional measurements such as we have it is not possible to unambiguously deter-

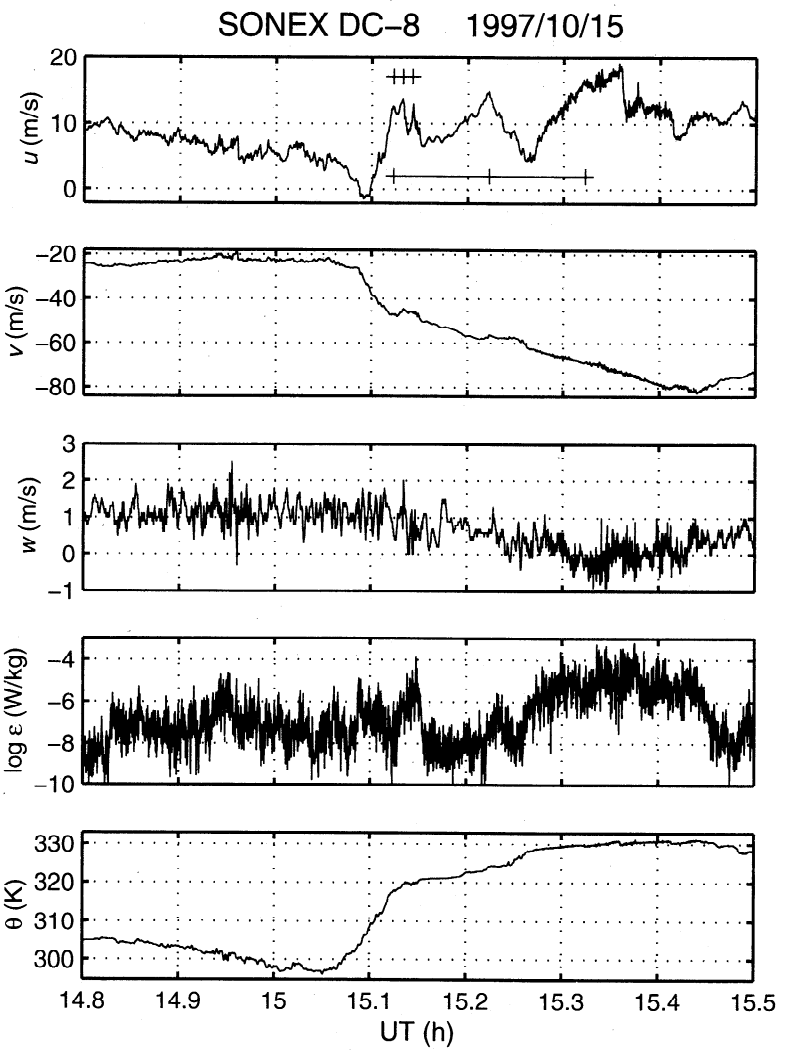

Figure 8. Plots, from top to bottom, of u, v, w, $\log\epsilon$, and θ through the two intersections with the western branch of the tropopause fold region on October 15, 1997. Suspected wave growth regions are marked on the u plot by horizontal bars and vertical tick marks. See text for explanation.

mine the wave parameters. Instead, we will focus again on the instabilities themselves and their effects on the ozone flux.

Figure 9 is a blowup plot of the second encounter with the tropopause fold. The oscillation was most clear in w, while smaller perturbations with the same period were also visible in θ, v, and, to a lesser extent, in ozone. The perturbations in u were not closely correlated to those in w, which is consistent with the plane of the vertical shear (estimated from the data to be 163°, measured clockwise from the north) being in closer alignment in the meridional direction than in the zonal direction.

Again, assuming that the oscillations were KH billows, we can estimate their horizontal wavelength and vertical thickness. Along the aircraft heading the period was ~25 s, which translates to a length of 5.2 km at the aircraft speed of 208 m s^{-1}. Since the aircraft heading was 82°, this yields a true horizontal wavelength of $\lambda_h = 5200\cos(163° - 82°) = 810$ m. The vertical thickness was then $\Delta z = \lambda_h/7.5 = 110$ m. These numbers are close to those from case 1.

One can readily see the mixing effects of the KH instability on the fold in the ozone measurement (Figure 9). The bottomside of the ozone maximum was much more diffuse than the topside. The ozone flux will be estimated shortly.

As in case 1, we can calculate N^2, the vertical shear, and Ri. These are shown in Figure 10. Again, there was a correspondence between regions of high shear and high thermal stability, conditions typically associated with KH instability. Ri did fall close to or below 0.25 during the period of the suspected KH billows (15.085–15.115 (1505:06–1506:54) UT), and, as with case 1, there was a region of negative N^2 (~15.14 (1508:24) UT) associated with a secondary ozone maxi-

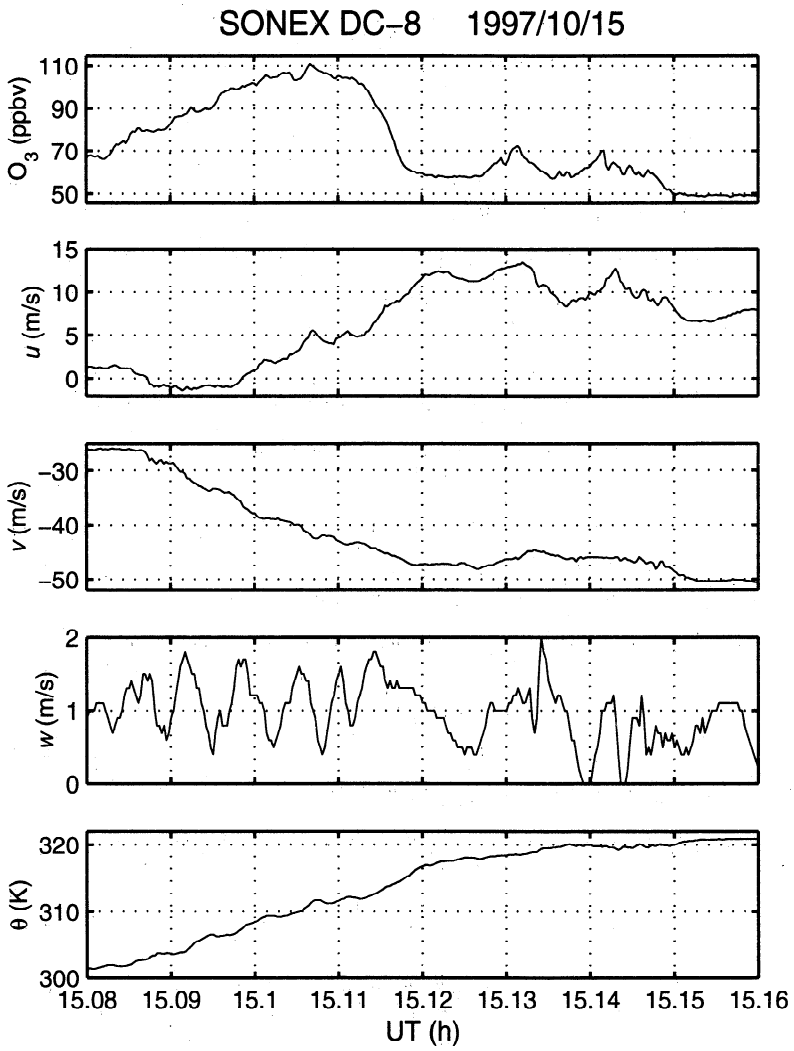

Figure 9. Expanded time plots, from top to bottom, of O_3, u, v, w, and θ from October 15, 1997.

mum and apparent wave breaking (as discussed above).

Finally, we estimate the vertical ozone flux for this period (Figure 11). Where $N^2 < 0$ ~15.15 (1509:00) UT, we took $|\Delta\theta| = 0.8$ K and $\Delta z = 80$ m for (4). The flux values are generally lower than for case 1. This is not surprising since the turbulence was weaker and the ozone gradients were smaller. Since the altitude of fold interception was lower in case 2 (~4 km) than in case 1 (~6.5 km), the stratospheric air inside the fold would have had more time to mix with the surrounding tropospheric air, thus weakening the ozone gradient at the edges. This can also be seen in the peak ozone concentration inside the folds, ~110 ppbv for case 2 versus ~190 ppbv for case 1. However, as in case 1, the estimated vertical ozone gradients of the substructures between 15.13 (1507:48) and 15.15 (1509:00) UT (and the corresponding fluxes) must be viewed with caution because of possible aliasing of horizontal gradients.

4. Summary Discussion

Even though the two cases of tropopause folding studied here occurred at different times and places and were sampled at different altitudes, there were some striking similarities. Both folds had sharply defined topsides with two foldlike substructures shortly following that contained lower ozone amounts than the fold itself. It is difficult to say whether these substructures were horizontal or vertical variations because the flight paths were one-dimensional and slantwise. Unfortunately, the near-field blind zone and coarse time resolution of the DIAL did not allow two-dimensional mapping of these small-scale ozone perturbations. If the perturbations were purely horizontal, then their separation distances would have been ~10 and 8 km for case 1 and case 2, respectively. If they were purely vertical, then their separation distances were ~400 and 200 m, respectively. Of

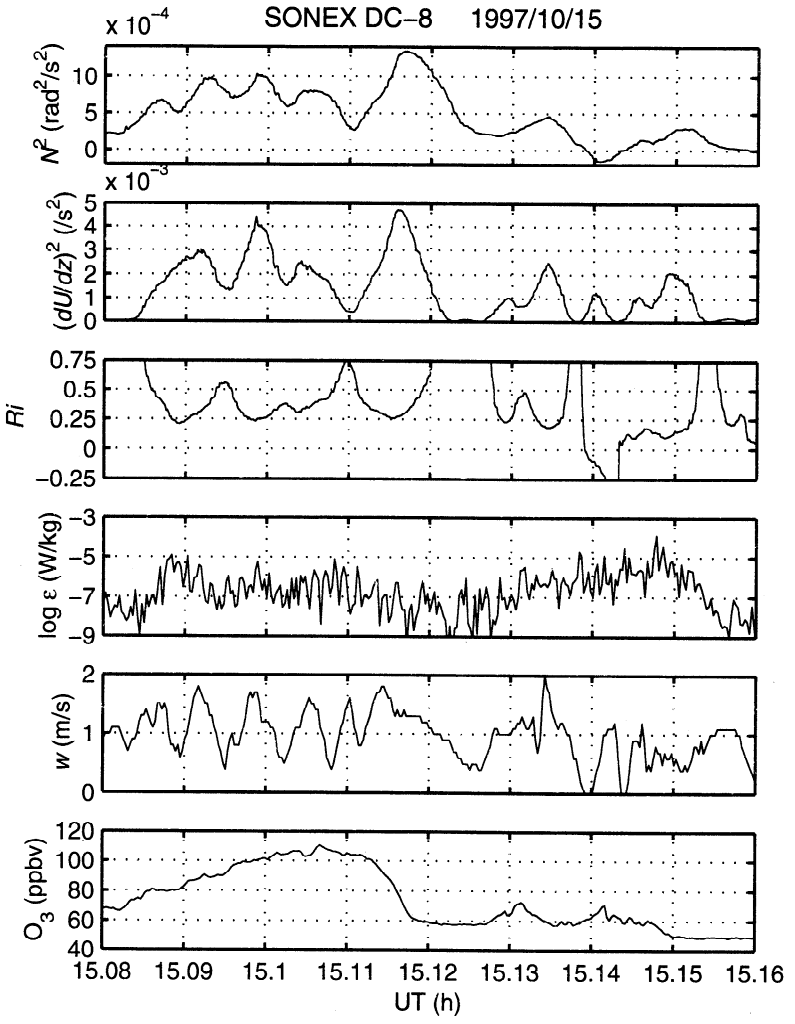

Figure 10. Plots, from top to bottom, of N^2, $(dU/dz)^2$, Ri, $\log\epsilon$, w, and O_3 mixing ratio from October 15, 1997.

course, the reality could have been somewhere in between the two extremes. Because in both cases the first of these substructures was associated with convective instability and turbulence and because there were wave-like perturbations in the wind and temperature corresponding to the ozone substructures, we proposed convectively breaking gravity waves to explain the data. It then follows that the substructures were mostly horizontal perturbations, since convective breakdown occurs in high-frequency gravity waves (KH instability sets in first for low-frequency gravity waves) [*Fritts and Rastogi*, 1985] and high-frequency gravity waves cannot have such short vertical wavelengths.

Although laboratory measurements and numerical studies confirm the existence of convective gravity wave breakdown, direct atmospheric observations have largely been lacking because of the difficulty in making the required high-resolution measurements. However, convective instability is believed to play a crucial role in gravity wave saturation [e.g., *Dunkerton*, 1989; *Fairall et al.*, 1991; *Andreassen et al.*, 1994]. Originally proposed by *Hodges* [1967], saturation theory calls for the natural growth of upward propagating gravity waves to be limited by various instabilities and/or diffusive damping/filtering mechanisms [e.g., *Gardner*, 1996]. Thus it is important to obtain more direct evidence that convective gravity wave breakdown does occur in the atmosphere and to pinpoint the conditions under which it proceeds. In this study we showed observational examples of convective gravity wave breaking, and for those cases the breaking appeared to occur preferentially just above a tropopause fold. This could be because the θ surfaces are moved farther apart vertically (thus weakening the static stability) on the cyclonic flank of a jet corresponding to where the tropopause fold is created [*Hoskins et al.*, 1985; *Price and Vaughan*, 1993]. Also, the rapid increase in horizontal velocity with height underneath the jet lowers the amplitude

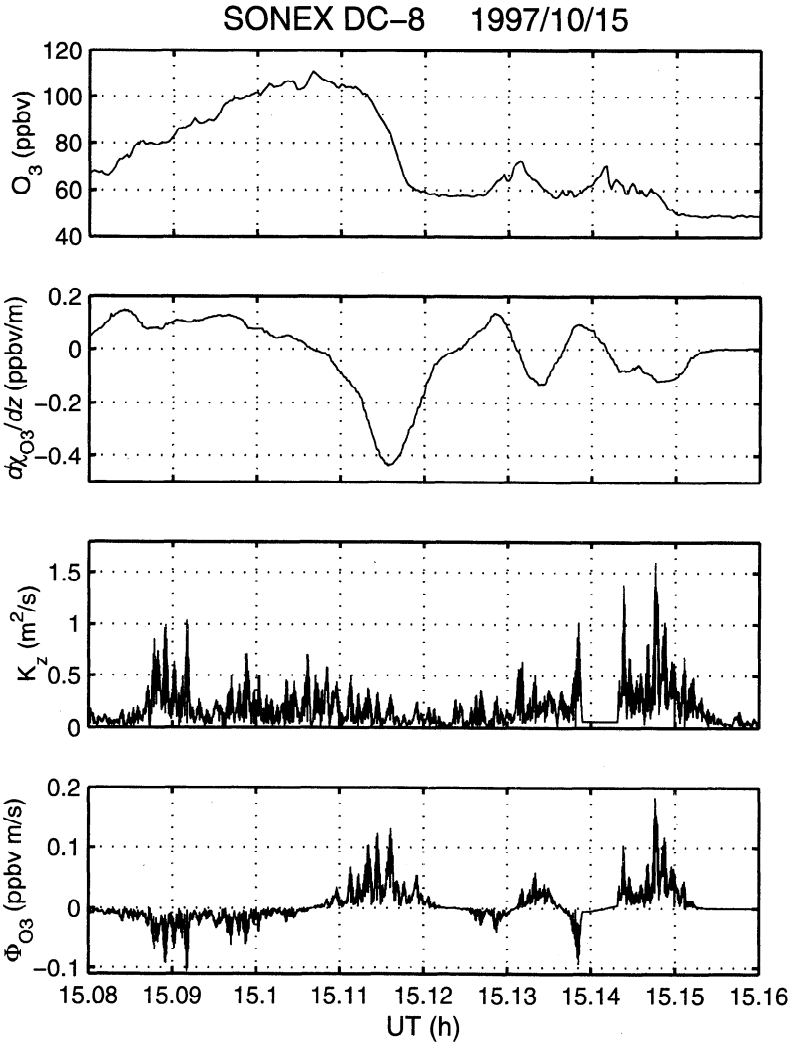

Figure 11. Plots, from top to bottom, of O_3 mixing ratio, vertical gradient of O_3 mixing ratio, K_z, and vertical flux of O_3 mixing ratio from October 15, 1997.

threshold for wave breaking [*Thorpe*, 1978] and causes more gravity waves with phase velocities in the same direction as the background flow to reach critical levels and convective instability [*Thorpe*, 1981; *Fritts*, 1982]. In any case, we need to add convectively breaking gravity waves to the list of mechanisms leading to the irreversible mixing of tropopause folds with their environment.

KH instabilities are much more commonly observed in the atmosphere (see, e.g., *Fritts and Rastogi* [1985] for references). We observed KH billows inside both tropopause folds encountered and noted a correlation between strong vertical shear and high static stability as anticipated theoretically [*Phillips*, 1966] and frequently observed [e.g., *Browning et al.*, 1973]. In case 2 the KH instability had apparently acted on the bottomside ozone gradient and made it much more diffuse than the topside of the fold, whereas in case 1 the KH instability located in the middle of the fold was not effective in mixing air inside and outside the fold.

The site of maximum ozone flux out of a tropopause fold was on the topside of case 1, with a peak value of $\sim$1.5 ppbv m s^{-1} in good agreement with previous aircraft observations by *Shapiro* [1980]. In this particular case the instability was generated by a combination of background shear and wave-induced weakening of static stability.

Acknowledgments. The work at MIT was funded by NASA grants NAG2-1105, NAG1-1758, and NAG1-1901. The work performed by M. J. Mahoney was carried out by the Jet Propulsion Laboratory, California Institute of Technology, under a contract with NASA. He also acknowledges the able assistance of Bruce L. Gary with the MTP data analysis. Finally, we would like to thank the DC-8 flight crew for their hard work.

References

Andreassen, Ø., C. E. Wasberg, D. C. Fritts, and J. R. Isler, Gravity wave breaking in two and three dimensions,

1, Model description and comparison of two-dimensional evolutions, *J. Geophys. Res.*, *99*, 8095–8108, 1994.

Appenzeller, C., H. C. Davies, and W. A. Norton, Fragmentation of stratospheric intrusions, *J. Geophys. Res.*, *101*, 1435–1456, 1996.

Browell, E. V., E. F. Danielsen, S. Ismail, G. L. Gregory, and S. M. Beck, Tropopause fold structure determined from airborne lidar and in situ measurements, *J. Geophys. Res.*, *92*, 2112–2120, 1987.

Browell, E. V., S. Ismail, and W. B. Grant, Differential absorption lidar (DIAL) measurements from air and space, *Appl. Phys. B*, *67*, 399–410, 1998.

Browning, K. A., G. W. Bryant, J. R. Starr, and D. N. Axford, Air motion within Kelvin-Helmholtz billows determined from simulaneous Doppler radar and aircraft measurements, *Q. J. R. Meteorol. Soc.*, *99*, 608–618, 1973.

Chan, K. R., J. Dean-Day, S. W. Bowen, and T. P. Bui, Turbulence measurements by the DC-8 meteorological measurement system, *Geophys. Res. Lett.*, *25*, 1355–1358, 1998.

Chapman, S., and T. G. Cowling, *The Mathematical Theory of Non-Uniform Gases*, 423 pp., Cambridge Univ. Press, New York, 1970.

Cho, J. Y. N., R. F. Jurgens, and M. A. Slade, High-resolution stratospheric dynamics measurements with the NASA/JPL Goldstone solar system radar, *Geophys. Res. Lett.*, *23*, 1909–1912, 1996.

Clough, P. N., and B. A. Thrush, Mechanism of chemiluminescent reaction between nitric oxide and ozone, *Trans. Faraday Soc.*, *63*, 915–925, 1967.

Collins, J. E., G. W. Sachse, B. E. Anderson, R. C. Harriss, K. B. Bartlett, S. T. Sandholm, L. O. Wade, L. G. Burney, and G. F. Hill, Airborne nitrous oxide observations over the western Pacific Ocean: September-October 1991, *J. Geophys. Res.*, *101*, 1975–1984, 1996.

Danielsen, E. F., and V. A. Mohnen, Project Duststorm report: Ozone transport, in situ measurements, and meteorological analyses of tropopause folding, *J. Geophys. Res.*, *82*, 5867–5877, 1977.

Danielsen, E. F., R. Bleck, J. Shedlovsky, A. Wartburg, P. Haagenson, and W. Pollock, Observed distribution of radioactivity, ozone, and potential vorticity associated with tropopause folding, *J. Geophys. Res.*, *75*, 2353–2361, 1970.

Danielsen, E. F., R. S. Hipskind, S. E. Gaines, G. W. Sachse, G. L. Gregory, and G. F. Hill, Three-dimensional analysis of potential vorticity associated with tropopause folds and observed variations of ozone and carbon monoxide, *J. Geophys. Res.*, *92*, 2103–2111, 1987.

Denning, R. F., S. L. Guidero, G. S. Parks, and B. L. Gary, Instrument description of the airborne microwave temperature profiler, *J. Geophys. Res.*, *94*, 16,757–16,766, 1989.

Dunkerton, T. J., Theory of internal gravity wave saturation, *Pure Appl. Geophys.*, *130*, 373–397, 1989.

Fairall, C. W., A. B. White, and D. W. Thomson, A stochastic model of gravity-wave-induced clear-air turbulence, *J. Atmos. Sci.*, *48*, 1771–1790, 1991.

Fritts, D. C., The transient critical-level interaction in a Boussinesq fluid, *J. Geophys. Res.*, *87*, 7997–8013, 1982.

Fritts, D. C., and T. J. Dunkerton, Fluxes of heat and constituents due to convectively unstable gravity waves, *J. Atmos. Sci.*, *42*, 549–556, 1985.

Fritts, D. C., and P. K. Rastogi, Convective and dynamical instabilities due to gravity wave motions in the lower and middle atmosphere: Theory and observations, *Radio Sci.*, *20*, 1247–1277, 1985.

Gardner, C. S., Testing theories of atmospheric gravity wave saturation and dissipation, *J. Atmos. Terr. Phys.*, *58*, 1575–1589, 1996.

Globe, S., and D. Dropkin, Natural convection heat transfer in liquids confined by two horizontal plates and heated from below, *J. Heat Transfer*, *81*, 156–185, 1959.

Hodges, R., Generation of turbulence in the upper atmosphere by internal gravity waves, *J. Geophys. Res.*, *72*, 3455–3458, 1967.

Hoskins, B. J., M. E. McIntyre, and A. W. Robertson, On the use and significance of isentropic potential vorticity maps, *Q. J. R. Meteorol. Soc.*, *111*, 877–946, 1985.

Ingersoll, A. P., Thermal convection with shear at high Rayleigh number, *J. Fluid Mech.*, *25*, 209–228, 1966.

Itsweire, E. C., K. N. Helland, and C. W. Van Atta, The evolution of grid-generated turbulence in stratified fluid, *J. Fluid Mech.*, *126*, 299–338, 1986.

Johnson, W. B., and W. Viezee, Stratospheric ozone in the lower troposphere, I, Presentation and interpretation of aircraft measurements, *Atmos. Environ.*, *15*, 1309–1323, 1981.

Kraichnan, R., Turbulent thermal convection at arbitrary Prandl number, *Phys. Fluids*, *5*, 1374–1389, 1962.

Langford, A. O., and S. J. Reid, Dissipation and mixing of a small-scale stratospheric intrusion in the upper troposphere, *J. Geophys. Res.*, *103*, 31,265–31,276, 1998.

Lilly, D. K., On the numerical simulation of buoyant convection, *Tellus*, *14*, 148–172, 1962.

Miles, J. W., and L. N. Howard, Note on a heterogeneous shear flow, *J. Fluid Mech.*, *20*, 331–336, 1964.

Orlanski, I., On the breaking of standing internal gravity waves, *J. Fluid Mech.*, *54*, 577–598, 1972.

Orlanski, I., and B. B. Ross, Numerical simulation of the generation and breaking of internal gravity waves, *J. Geophys. Res.*, *78*, 8808–8826, 1973.

Phillips, O. M., *The Dynamics of the Upper Ocean*, 261 pp., Cambridge Univ. Press, New York, 1966.

Price, J. D., and G. Vaughan, On the potential for stratosphere-troposphere exchange in cut-off low systems, *Q. J. R. Meteorol. Soc.*, *119*, 343–365, 1993.

Priestley, C. H. B., Convection from a horizontal surface, *Aust. J. Phys.*, *7*, 176–201, 1954.

Sachse, G. W., G. F. Hill, L. O. Wade, and M. G. Perry, Fast-response, high precision carbon monoxide sensor using a tunable diode laser absorption technique, *J. Geophys. Res.*, *92*, 2071–2081, 1987.

Shapiro, M. A., A multiple-structured frontal zone-jet stream system as revealed by meteorologically instrumented aircraft, *Mon. Weather Rev.*, *102*, 244–253, 1974.

Shapiro, M. A., Turbulent mixing within tropopause folds as a mechanism for the exchange of chemical constituents between the stratosphere and troposphere, *J. Atmos. Sci.*, *37*, 994–1004, 1980.

Singh, H. B., A. M. Thompson, and H. Schlager, SONEX airborne mission and coordinated POLINAT-2 activity: Overview and accomplishments, *Geophys. Res. Lett.*, in press, 1999.

Thorpe, S. A., On the shape and breaking of finite amplitude gravity waves in a shear flow, *J. Fluid Mech.*, *85*, 7–31, 1978.

Thorpe, S. A., An experimental study of critical layers, *J. Fluid Mech.*, *103*, 321–344, 1981.

Walterscheid, R. L., and G. Schubert, Nonlinear evolution of an upward propagating gravity wave: Overturning, convection, transience and turbulence, *J. Atmos. Sci.*, *47*, 101–125, 1990.

Weinstock, J., On the theory of turbulence in the buoyancy subrange of stably stratified flows, *J. Atmos. Sci.*, *35*, 634–649, 1978.

Weinstock, J., Vertical diffusivity and overturning length in stably stratified turbulence, *J. Geophys. Res.*, *97*, 12,653–12,658, 1992.

E. V. Browell, G. L. Gregory, G. W. Sachse, and S. A. Vay, NASA Langley Research Center, Hampton, VA 23681-2199. (e.v.browell@larc.nasa.gov; g.l.gregory@larc.nasa.gov; g.w.sachse@larc.nasa.gov; s.a.vay@larc.nasa.gov)

T. P. Bui, Mail Stop 245-5, NASA Ames Research Center, Moffett Field, CA 94035-1000. (bui@mms.arc.nasa.gov)

J. Y. N. Cho and R. E. Newell, Department of Earth, Atmospheric, and Planetary Sciences, Massachusetts Institute of Technology, 77 Massachusetts Ave., 54-1823, Cambridge, MA 02139-4307. (jcho@pemtropics.mit.edu; newell@newell1.mit.edu)

M. A. Fenn, Science Applications International Corporation, 1 Enterprise Parkway, Hampton, VA 23666. (m.a.fenn@larc.nasa.gov)

T. L. Kucsera and A. M. Thompson, Code 916, NASA Goddard Space Flight Center, Greenbelt Rd., Greenbelt, MD 20771-0001. (tlk@croc.gsfc.nasa.gov; thompson@gator1.gsfc.nasa.gov)

M. J. Mahoney, Mail Stop 246-101, NASA Jet Propulsion Laboratory, California Institute of Technology, 4800 Oak Grove Dr., Pasadena, CA 91109-8099. (michael.j.mahoney@jpl.nasa.gov)

(Received January 14, 1999; revised May 25, 1999; accepted June 16, 1999.)